ARTICLE

# Quantum Entanglement of Parallel-Coupled Double Quantum Dots: a Theoretical Study Using the Hierarchical Equations of Motion Approach†

Hong Gong[a], Arif Ullah[a], LvZhou Ye[a], Xiao Zheng[a]*, YiJing Yan[b]

*a. Hefei National Laboratory for Physical Sciences at the Microscale & Synergetic Innovation Center of Quantum Information and Quantum Physics, University of Science and Technology of China, Hefei 230026, China*

*b. Hefei National Laboratory for Physical Sciences at the Microscale & iChEM, University of Science and Technology of China, Hefei 230026, China*

(Dated: Received on June 11, 2018; Accepted on July 12, 2018)

Quantum dots comprise a type of quantum impurity system. The entanglement and coherence of quantum states are significantly influenced by the strong electron-electron interactions among impurities and their dissipative coupling with the surrounding environment. Competition between many-body effects and transfer couplings plays an important role in determining the entanglement among localized impurity spins. In this work, we employ the hierarchical-equations-of-motion approach to explore the entanglement of a strongly correlated double quantum dots system. The relation between the total system entropy and those of subsystems is also investigated.

**Key words:** Double quantum dots, Quantum entanglement, Rényi entropy, von Neumann entropy, Concurrence, Hierarchical-equations-of-motion method

## I. INTRODUCTION

Entanglement is one of the marvelous features of quantum mechanics. It describes nonlocal correlation between different quantum objects. From information perspective, entanglement can be used in quantum computation and quantum information storing applications [1]. Moreover, entanglement can be experimentally quantified. In 2015, Islam *et al.* prepared and interfered two identical copies of a four-site Bose-Hubbard system, and measured the entanglement [2], in terms of the Rényi entropy and mutual information [3]. In 2017, Cocchi *et al.* measured the entropy and short-range correlations in a two-dimensional Hubbard system [4]. Generally speaking, quantum computation applications rely greatly on the generation, control, and detection of entangled states [5].

Double quantum dots (DQDs) comprise one of the fundamental and relatively simple open quantum systems. The physics of DQDs is intriguing and fundamental, including the many-body characteristic Kondo phenomena [6–9]. Besides the practical applications in nanoelectronics, DQDs also play a vital role in quantum information processing [10–12], and have been used in implementing two-electron spin entanglement [13]. Furthermore, entanglement of DQDs can be used to convey quantum information through a computing device [1].

There are some theoretical studies on entanglement in DQDs [9, 14, 15]. However, the underlying mechanism, especially the strong correlation many-body effects on entanglement, remains a challenging task. Therefore, an accurate and universal approach capable of addressing strong correlation effects on entanglement in DQDs is highly desirable. Various methods have been used to study the entanglement of DQDs. Ramšak *et al.* have applied the numerical renormalization group method to study the competition between pair entanglement of two spin qubits in DQDs with various topologies [14]. Büsser *et al.* have employed the time-dependent density matrix renormalization group method to a DQD Aharonov-Bohm interferometer system [9]. They demonstrated that an entangled charge state can be induced and controlled by sending an electrical current through the structure [9].

In this work, we exploit the hierarchical-equations-of-motion (HEOM) approach [16]. This is a nonperturbative method for combined effects of system-reservoir dissipation, non-Markovian memory and electron-electron interactions. It has been applied to investigate a wide range of equilibrium and nonequilibrium, static and dynamic properties of quantum dot systems [17–23]. The resultant reduced and auxiliary density matrices and their dynamical responses contain rich quantum phenomena, including entanglements and strong many-body correlations. By using the HEOM method, Hou

†Part of the special issue for celebration of "the 60th Anniversary of University of Science and Technology of China and the 30th Anniversary of Chinese Journal of Chemical Physics".

*Author to whom correspondence should be addressed.
E-mail: xz58@ustc.edu.cn

 

*et al.* demonstrated that quantum phase has critical influence on quantum entanglement in Aharonov-Bohm double quantum dot (DQD) interferometer [20]. The present work aims at characterizing entanglement in parallel-coupled DQDs, with the HEOM calculations on various related quantities. The interplay between entanglement and many-body phenomena will be analyzed.

A concise illustration of the parallel-coupled DQD model is given. The HEOM approach is employed to evaluate various quantities that quantify entanglement. We demonstrate that the resultant entanglement is mainly determined by the spin-spin correlation.

## II. MODEL AND METHODOLOGY

### A. Two-impurity Anderson model

With the second quantization formulation, the system Hamiltonian is expressed with the creation and annihilation operators, $\{\hat{a}^\dagger_{\nu s}\}$ and $\{\hat{a}_{\nu s}\}$, of the system electrons. These operators are represented by $m\times m$ matrices, with $m$ being the number of Fock states that span the system Hilbert space. For a spin resolved single impurity, the system Hilbert space is spanned by four Fock states: the vacant $|0\rangle$, the singly occupied $|\uparrow\rangle$ and $|\downarrow\rangle$ by individual spin-up and spin-down electrons, and the doubly occupied $|d\rangle$.

We adopt the two-impurity Anderson model (TIAM) [24], to represent the DQD of interest in this work. The localized spins are considered to be magnetic impurities, which interact with its surrounding environment. The system, with the two subsystems A and B, is in parallel transport setup, as sketched in FIG. 1.

The total Hamiltonian consists of the DQD impurity system ($H_{\rm sys}$), the electrons reservoirs leads ($H_{\rm leads}$), and their couplings ($H_{\rm coup}$). The system Hamiltonian is

$$H_{\rm sys}=\sum_{i={\rm A,B}}\big[\epsilon_i(\hat{n}_{i\uparrow}+\hat{n}_{i\downarrow})+U_i\hat{n}_{i\uparrow}\hat{n}_{i\downarrow}\big]+\big[t_{\rm AB}\big(\hat{a}^\dagger_{{\rm A}\uparrow}\hat{a}_{{\rm B}\uparrow}+\hat{a}^\dagger_{{\rm A}\downarrow}\hat{a}_{{\rm B}\downarrow}\big)+H.c.\big] \quad (1)$$

Here, $H.c.$ stands for the Hermitian conjugate. Each dot ($i$=A or B) contributes one spin-degenerate orbital level to the transport, with energy $\epsilon_{i\uparrow}=\epsilon_{i\downarrow}=\epsilon_i$. In Eq.(1), $\hat{a}^\dagger_{is}$ ($\hat{a}_{is}$) denotes the creation (annihilation) operator for an electron on the spin specified orbital, and $\hat{n}_{is}=\hat{a}^\dagger_{is}\hat{a}_{is}$ is the occupation number operator, $U_{\rm A}=U_{\rm B}=U$ is the intradot Coulomb interaction strength, $t_{\rm AB}$ is the interdot transfer coupling strength. The electrons in two reservoirs leads, $\alpha$=L and R, are described by

$$H_{\rm leads}=\sum_{\alpha ks}\epsilon_{\alpha k}\hat{d}^\dagger_{\alpha ks}\hat{d}_{\alpha ks} \quad (2)$$

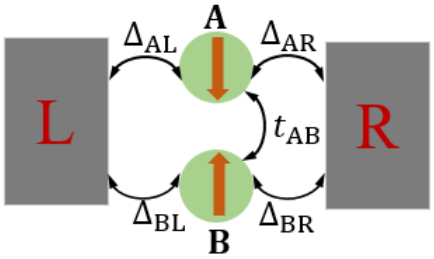


FIG. 1 The parallel-coupled DQD system described by two-impurity Anderson model (TIAM). The two dots are labeled by $i$=A and B, with the spin-independent transfer coupling strength $t_{\rm AB}$. The up and down arrows at dots A and B indicate an effective antiferromagnetic interdot interaction induced by $t_{\rm AB}$; see the text for details. The two leads are denoted by $\alpha$=L and R. The dot-lead coupling strengths $\Delta_{i\alpha}$ have the same value in our model.

where $\hat{d}^\dagger_{\alpha ks}$ ($\hat{d}_{\alpha ks}$) creates (annihilates) an electron on the $k$th state of energy $\epsilon_{\alpha k}$. The interactions between dots and leads are described by the transfer coupling Hamiltonian,

$$H_{\rm coup}=\sum_{\alpha iks}t_{\alpha ik}\,\hat{a}^\dagger_{is}\,\hat{d}_{\alpha ks}+\ H.c. \quad (3)$$

where $\{t_{\alpha ik}\}$ are the coupling constants. The influence of leads on the dots is characterized by the hybridization function, $\Delta_{\alpha,ij}(\omega)\equiv\pi\sum_k t_{\alpha ik}\,t^*_{\alpha jk}\,\delta(\omega-\epsilon_{\alpha k})$. In this work, it assumes the Lorentzian form,

$$\Delta_{\alpha,ij}(\omega)=\delta_{ij}\frac{\Delta_\alpha}{2}\frac{W^2}{(\omega-\mu_\alpha)^2+W^2} \quad (4)$$

Here, $\mu_\alpha$ is the chemical potential of $\alpha$-lead, $W$ is the band width, and $\Delta_\alpha$ is the coupling strength. The overall dot-lead coupling strength, $\Delta=\sum_\alpha\Delta_\alpha$, is taken to be the energy unit hereafter. The above TIAM model has been realized experimentally in DQD systems, with the interdot coupling strength tunable by plunger gates [25].

### B. Measures of entanglement

Let $\rho_{\rm AB}$ be the reduced double-dots system density matrix. One can assign it a state on the subsystem A by

$$\rho_{\rm A}={\rm tr}_{\rm B}(\rho_{\rm AB}) \quad (5)$$

where ${\rm tr}_{\rm B}$ is partial trace with respect to subsystem B. This is the reduced density matrix of the subsystem dot A, and that of the dot B is defined similarly and denoted as $\rho_{\rm B}={\rm tr}_{\rm A}(\rho_{\rm AB})$. Apparently, $\rho_{\rm AB}=\rho_{\rm A}\otimes\rho_{\rm B}$, if and only if the subsytems A and B are uncorrelated.

DOI:10.1063/1674-0068/31/cjcp1806138 

The quantum entanglement considered in this work refers to the nonclassical and nonlocal correlation between subsystems A and B. Obviously, $\rho_{\rm AB}\neq\rho_{\rm A}\otimes\rho_{\rm B}$ if A and B are entangled.

There have been several physical quantities used for the measure of quantum entanglement [1]. Entropy of entanglement is an entanglement measure for a many-body quantum state. It plays a significant role in quantum information. The smaller the entropy, the stronger the entanglement. Two kinds of entropy will be employed to measure the bipartite entanglement between the two dots. One is the von Neumann entropy [26],

$$\mathcal{S}_{{\rm vN}(\rho)} = -{\rm tr}(\rho\ln\rho) \tag{6}$$

The von Neumann entropy can be viewed as the quantum version of the classical Shannon entropy in information theory [27]. For a quantum system, $\mathcal{S}_{\rm vN}$ quantifies how far the system state departs from a pure state.

Another entropy is the Rényi entropy [28], which is a generalization of the von Neumann entropy. Note that the Rényi entropy differs in general from thermodynamic entropy [29]. The latter is given by Boltzmann, *i.e.*, $\mathcal{S}=k_{\rm B}\ln\Omega$, with $\Omega$ being the number of microstates that correspond to the macroscopic thermodynamic states and $k_{\rm B}$ is the Boltzmann constant.

The Rényi entropy of order $n$ (with $n>0$), $\mathcal{S}_n(\rho)$, is defined as [28]

$$\mathcal{S}_n(\rho) = \frac{1}{1-n}\ln{\rm tr}(\rho^n) \quad (n\neq1) \tag{7}$$

Apparently, Rényi entropy provides a continuous spectrum of entanglement measure parameterized by variable $n$.

Specifically, the zeroth-order Rényi entropy, $\mathcal{S}_0(\rho)=\ln m$, is also called the Hartley entropy or maximum entropy [30], where $\rho$ is an $m\times m$ matrix. Here, $m=(2N_s)^{N_\nu}$ for a general impurity of $N_\nu$ orbitals, and $N_s=2$ in the spin-resolved scenario. In the limit of $n\to1$, the Rényi entropy recovers the von Neumann entropy [28]:

$$\mathcal{S}_{\rm vN}(\rho) = \lim_{n\to1}\mathcal{S}_n(\rho) = \mathcal{S}_1(\rho) \tag{8}$$

For consistency the von Neumann entropy will be denoted as $\mathcal{S}_1(\rho)$. The second-order Rényi entropy, $\mathcal{S}_2(\rho)=-\ln{\rm tr}(\rho^2)$, is also called the collision entropy [28].

The Rényi entropy of order $n$ is non-negative. It is a monotonic function and there exist inequalities between different values of $n$, $\mathcal{S}_0(\rho)\geq\mathcal{S}_1(\rho)\geq\mathcal{S}_2(\rho)$ [31]. The Rényi entropy satisfies the triangle inequality [1],

$$|\mathcal{S}_n({\rm A})-\mathcal{S}_n({\rm B})| \leq \mathcal{S}_n({\rm AB}) \leq \mathcal{S}_n({\rm A})+\mathcal{S}_n({\rm B}) \tag{9}$$

Denote for simplicity hereafter $\mathcal{S}_n({\rm A})\equiv\mathcal{S}_n(\rho_{\rm A})$, $\mathcal{S}_n({\rm B})\equiv\mathcal{S}_n(\rho_{\rm B})$, and $\mathcal{S}_n({\rm AB})\equiv\mathcal{S}_n(\rho_{\rm AB})$. As the two dots considered in this work are equivalent, we have $\mathcal{S}_n({\rm A})=\mathcal{S}_n({\rm B})$.

As for the measure of correlation between quantum subsystems, we exploit the quantum mechanical analog of the Shannon mutual information [3],

$$I_n({\rm A},{\rm B}) = \mathcal{S}_n({\rm A})+\mathcal{S}_n({\rm B})-\mathcal{S}_n({\rm AB}) \tag{10}$$

This measures the shared mutual information between systems A and B, and represents a quantitative description for the physical amount of quantum correlation. Mutual information exhibits interesting scaling properties with respect to subsystem size, which plays a vital role in studying the area laws [32] in interacting quantum systems [33].

It is well known that at low temperature the parallel-coupled DQDs exhibit conspicuous Kondo effect [6, 7, 9]. Kondo states originate from the screening of local magnetic moment on the dots by itinerary electrons in the leads, and they reflect the entanglement between DQDs and leads. However, the reduced system density matrix $\rho$ characterizes mostly the entanglement between the two dots. Therefore, the Kondo states in the DQD system would have rather minor influence on the above defined entropies.

On the other hand, the interdot coupling $t_{\rm AB}$ gives rise to an effective antiferromagnetic (AFM) interaction between the local spin moments on the two dots [15, 34, 35]. Such an AFM interaction plays a dominant role in the entanglement between the two dots when $t_{\rm AB}$ is large. To quantify the relation between the quantum entanglement and the strength of AFM interaction, we also examine the concurrence $C_{\rm AB}$ (see Eq.(11)). This quantity measures the entanglement between the two dots from the perspective of spin-spin correlation [20, 36].

The spin operator associated with the $\nu$th dot is constructed as $\hat{\boldsymbol{S}}_\nu=\frac{1}{2}\sum_{ss'}\hat{a}^\dagger_{\nu s}\boldsymbol{\sigma}_{ss'}\hat{a}_{\nu s'}$, where $\boldsymbol{\sigma}$ represents the vector of Pauli matrices. For the DQD, the total spin moment is $\langle S^2\rangle=S(S+1)$ for a pure spin-state. The total spin number of a DQD is either $S=0$ (singlet, $M_S=0$) or $S=1$ (triplet, $M_S=0,\pm1$). Moreover, the spin correlation between the two dots is evaluated by $S_{\rm AB}=\langle\hat{\boldsymbol{S}}_{\rm A}\cdot\hat{\boldsymbol{S}}_{\rm B}\rangle$. It is well known that $S_{\rm AB}=1/4$ for the two electrons forming a triplet, and $S_{\rm AB}=-3/4$ for a spin singlet. Realistic DQD is in a mixed spin-state. An ideal mixture acquires the values of $\langle S^2\rangle=0.75\langle S^2\rangle^{\rm triplet}+0.25\langle S^2\rangle^{\rm singlet}=3/2$ and $S_{\rm AB}=0$. Physically, $S_{\rm AB}<0$ and $S_{\rm AB}>0$ represent the effective antiferromagnetic and ferromagnetic interdot interactions, respectively.

The concurrence $C_{\rm AB}$ is determined via the reduced system-spin density matrix as [36]

$$C_{\rm AB} = \max\left(0,\sqrt{\lambda_1}-\sqrt{\lambda_2}-\sqrt{\lambda_3}-\sqrt{\lambda_4}\right) \tag{11}$$

with $\lambda_1,\cdots,\lambda_4$ denoting the decreasing-ordered eigenvalues of the nonnegative Hermitian matrix $R=\rho_s\tilde{\rho}_s$. Here, $\tilde{\rho}_s=(\sigma_y\otimes\sigma_y)\rho^*_s(\sigma_y\otimes\sigma_y)$, and $\rho_s$ is the specified $4\times4$ submatrix of $\rho_{\rm AB}$, spanning over the bi-occupation

DOI:10.1063/1674-0068/31/cjcp1806138 

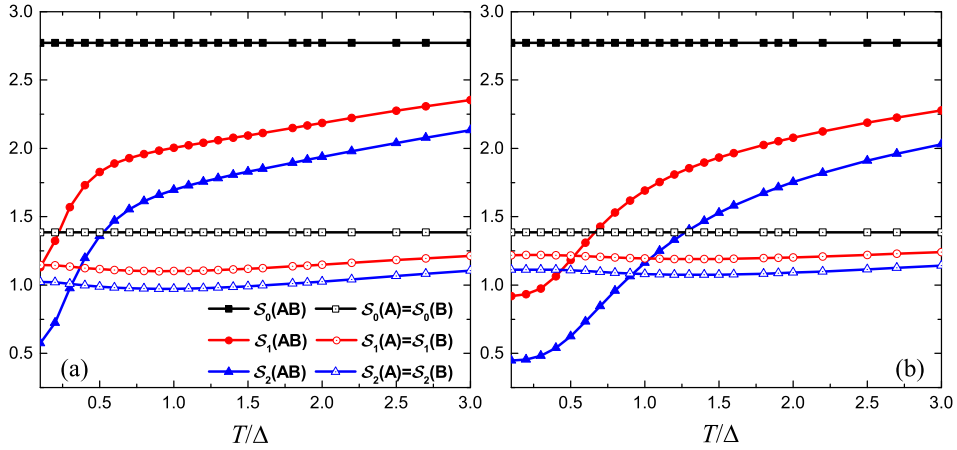


FIG. 2 Rényi entropy $\mathcal{S}_n$ of system and subsystems, as a function of temperature $T$, with (a) $t_{\rm AB}$=1.5 $\Delta$ and (b) $t_{\rm AB}$=2.5 $\Delta$. See text for other parameters.

Fock states, $|\uparrow\uparrow\rangle$, $|\uparrow\downarrow\rangle$, $|\downarrow\uparrow\rangle$, and $|\downarrow\downarrow\rangle$, over two dots. Because there is no direct spin-flip term in the system Hamiltonian (Eq.(1)), the concurrence Eq.(11) can be related to $S_{\rm AB}$ via [9]

$$C_{\rm AB} = \max\left\{0, -\frac{1}{2} - \frac{2S_{\rm AB}}{\hat{N}^s_{\rm A}\hat{N}^s_{\rm B}}\right\} \qquad (12)$$

Here $\hat{N}^s_\nu$=$\hat{n}_{\nu\uparrow}$+$\hat{n}_{\nu\downarrow}$−2$\hat{n}_{\nu\uparrow}\hat{n}_{\nu\downarrow}$. To ensure the same value of $C_{\rm AB}$ being obtained by Eqs. (11) and (12), the submatrix $\rho_s$ needs to be normalized by $\langle\hat{N}^s_1\hat{N}^s_2\rangle$ [37]. Whenever there are entangled states, $C_{\rm AB}$>0; otherwise, $C_{\rm AB}$=0 indicates that there is no entanglement.

## III. RESULTS AND DISCUSSION

In the following, we employ the HEOM–QUICK program [23] to calculate the reduced system density matrix $\rho_{\rm AB}$ of the DQDs. The DQD systems are considered in equilibrium. The truncation tier is set to be $L$=4. It is sufficient to yield quantitatively converged results for weak and medium dot-lead coupling considered in this work. The resultant Rényi entropy $\mathcal{S}_n$ (Eqs. (7) and (6)), the quantum mutual information $I_n$(A, B) (Eq.(10)), and the concurrence $C_{\rm AB}$ (Eq.(12)), are then reported. In all calculations, we set the parameters (in units of $\Delta$) $W$=10, $U_{\rm A}$=$U_{\rm B}$=10, and $\epsilon_{\rm A}$=$\epsilon_{\rm B}$=−5. The interdot coupling strength $t_{\rm AB}$ and temperature $T$ are variables.

FIG. 2 reports various Rényi entropies, $\mathcal{S}_n$(AB) and $\mathcal{S}_n$(A)=$\mathcal{S}_n$(B), as a function of temperature $T$, at two values of interdot coupling strength $t_{\rm AB}$=1.5 $\Delta$ and $t_{\rm AB}$=2.5 $\Delta$. Each individual DQD system entropy $\mathcal{S}_{n>0}$(AB) increases as temperature increases. This corresponds to the entanglement reduction. Non-local correlation and entanglement are mainly limited to low temperature region ($T$<0.5 $\Delta$). On the other hand, the entropy of individual dot, $\mathcal{S}_{n>0}$(A)=$\mathcal{S}_{n>0}$(B), is

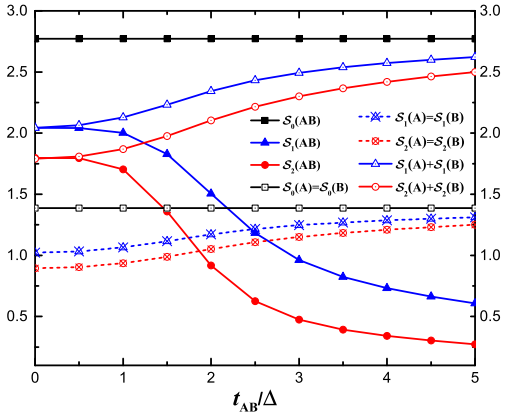


FIG. 3 Rényi entropy $\mathcal{S}_n$ of system and subsystems as function of interdot coupling strength $t_{\rm AB}$, at $T$=0.5 $\Delta$. See text for other parameters.

rather insensitive to $T$, since the dot's internal structure has little correlation with temperature. It is also observed that the stronger coupling intensity $t_{\rm AB}$ is, the smaller the $\mathcal{S}_n$(AB) will be, indicating the entanglement is stronger. Note that the maximum entropies are of $\mathcal{S}_0$(AB)=2$\mathcal{S}_0$(A)=2$\mathcal{S}_0$(B)=ln16≈2.77, that depend only on the system size, but not on the temperature and interdot coupling strength.

FIG. 3 depicts the Rényi entropies as functions of interdot coupling strengths $t_{\rm AB}$, at temperature $T$=0.5 $\Delta$. At $t_{\rm AB}$=0, $\mathcal{S}_n$(AB)=$\mathcal{S}_n$(A)+$\mathcal{S}_n$(B), indicating the subsystems A and B are not entangled in this trivial case. The subsystems will remain unentangled in the weak $t_{\rm AB}$ regime. It requires a certain minimum nonzero $t_{\rm AB}$, giving rise to antiferromagnetic correlation, for the two spins to be entangled.

The evaluated entropies satisfy the triangle inequality, Eq.(9). The second-order Rényi entropy, $\mathcal{S}_2$, provides the lower bound [31] to the von Neumann entropy, $\mathcal{S}_1$=$\mathcal{S}_{\rm vN}$. While the later has been used ex-

DOI:10.1063/1674-0068/31/cjcp1806138 

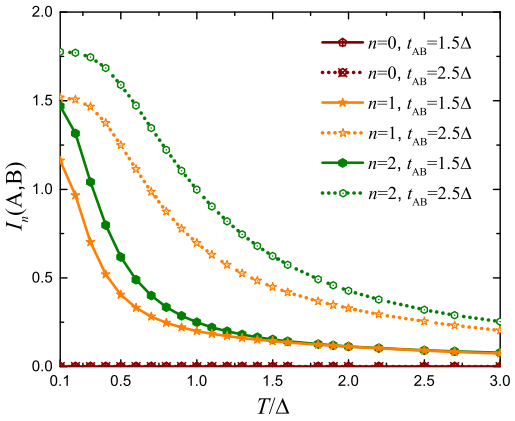


FIG. 4 Quantum mutual entropy $I_n(\mathrm{A,B})$ as a function of temperature $T$, at the specified values of $t_{\mathrm{AB}}$. See text for other parameters.

tensively in various context, $\mathcal{S}_2$ is used to specify the sufficient conditions of entanglement: $\mathcal{S}_2(\mathrm{A})>\mathcal{S}_2(\mathrm{AB})$ and $\mathcal{S}_2(\mathrm{B})>\mathcal{S}_2(\mathrm{AB})$ [38, 39]. From FIG. 3, such inequalities become true at $t_{\mathrm{AB}}>1.8\ \Delta$. These entropic inequalities are more powerful in detecting certain entangled states than other inequalities such as the Clauser-Horne-Shimony-Holt inequality [39, 40]. Evidently, strong entanglement occurs in the strong coupling strength regime.

FIG. 4 shows the quantum mutual entropy, $I_n$(A,B) of Eq.(10), as a function of temperature. Thermal fluctuation suppresses the quantum correlation effect. The classical characteristics emerges gradually as the temperature increases. At higher temperature, the mutual information approaches to zero, indicating the absence of any correlation. Non-local correlation and entanglement are mainly limited in the low temperature region ($T<0.5\ \Delta$), which agrees with that of FIG. 2.

As discussed earlier, we would like to link the total spin moment $\langle S^2\rangle$ and the spin correlation $S_{\mathrm{AB}}$, with the measure of entanglement in terms of the concurrence $C_{\mathrm{AB}}$. In FIG. 5 and FIG. 6, we plot these quantities as functions of interdot coupling strength $t_{\mathrm{AB}}$ (left-panels) and of temperature $T$ (right-panels) respectively. Remarkably, nonzero $C_{\mathrm{AB}}$ occurs only with sufficiently large $t_{\mathrm{AB}}$ or at low temperature (see FIG. 5). Evidently, the entanglement-on characteristics depends sensitively on both $t_{\mathrm{AB}}$ and $T$. As shown in FIG. 6(a), the switch-on value of $t_{\mathrm{AB}}$ decreases as the temperature decreases. One would expect an elevation of the switch-on value of $T$ as the interdot coupling $t_{\mathrm{AB}}$ increases. However, it is not the case as shown in FIG. 6(b). The concurrence $C_{\mathrm{AB}}$ in the inset there switches on at $T\approx1.5\ \Delta$ when $t_{\mathrm{AB}}=1.5\ \Delta$, but at a depressed temperature of $T\approx0.7\ \Delta$, when the interdot coupling increases to $t_{\mathrm{AB}}=2.5\ \Delta$. The interplay between the interdot-spin correlations and the itinerant electrons induced screening effect on entanglement would be anticipated, as follows.

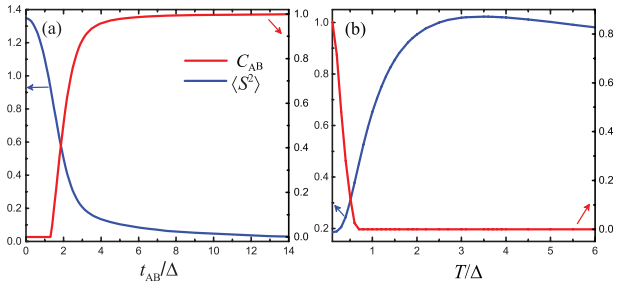


FIG. 5 The total spin moment $\langle S^2\rangle$ and the concurrence $C_{\mathrm{AB}}$, versus (a) the inter-dot coupling strength $t_{\mathrm{AB}}$ for temperature $T$=0.5 Δ and (b) the temperature $T$ at $t_{\mathrm{AB}}$=2.5 Δ. See text for other parameters.

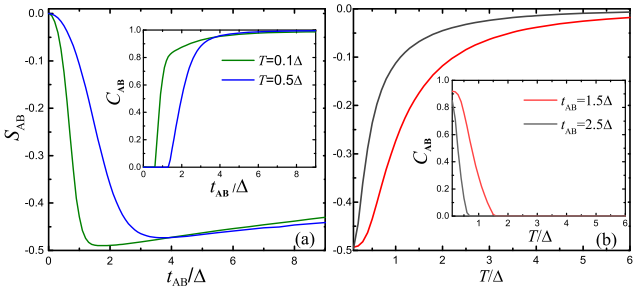


FIG. 6 The spin correlation $S_{\mathrm{AB}}$ versus (a) the interdot coupling strength $t_{\mathrm{AB}}$ and (b) the temperature $T$. Each inset depicts the corresponding concurrence $C_{\mathrm{AB}}$ at specified values of $T$ or $t_{\mathrm{AB}}$. See text for other parameters.

First of all, in the presence of itinerant electrons, the actual state should be a mixture of singlet and triplet states. This is supported by the fact that $0<\langle S^2\rangle<2$, exclusively between the values of the two pure spin-states. When $t_{\mathrm{AB}}$ is smaller than a critical value, and/or the screening effect would be dominant on individual dot, the two dots tend to form an artificial molecule through a combination similar to ionic bond [41]. Under the influence of $t_{\mathrm{AB}}$, electrostatic redistribution occurs within each dot, therefore resulting in an attractive Coulomb interaction between two dots. The two spin moments are nearly independent of each other, and the local spin at each dot is separately screened by itinerant electrons. As a result, there can be no entanglement between electrons on the dots.

When $t_{\mathrm{AB}}$ is larger than a certain critical value, the electrons in the dots are coherently coupled together, causing the dots to form an artificial molecule through a bonding similar to covalent bond [41]. At $T$=0.5 Δ, the total spin moment $\langle S^2\rangle$ is 3/4 while the interdot coupling strength $t_{\mathrm{AB}}$ takes the value of 1.55 Δ. The local spin at one dot is totally screened by itinerant electrons, this yields an $S$=1/2 residual spin. One can see the concurrence $C_{\mathrm{AB}}$ has a large rise over the range of $1.55\ \Delta<t_{\mathrm{AB}}<3\ \Delta$, corresponding to an abruptly increased entanglement between two dots. Low negative value of spin correlation indicates that electrons local-

DOI:10.1063/1674-0068/31/cjcp1806138 

ized in the dots have high probability to form a spin singlet.

As $t_{\rm AB}$ increases, $\langle S^2\rangle$ decreases and finally approaches to zero; on the contrary, $C_{\rm AB}$ increases and finally reaches the value of one. Electrons in the dots form an entangled spin singlet. Although $C_{\rm AB}$ and $\langle S^2\rangle$ change slowly, entanglement still becomes stronger. The results agree well with the conclusions we get from FIG. 3.

From FIG. 6(a), it can be observed that, with the increase of $t_{\rm AB}$, the entanglement is always increasing; but the spin correlation $S_{\rm AB}$ has a minimal negative value versus a critical $t_{\rm AB}$. In other words, there exists a maximal AFM interaction, corresponding to a strong entanglement.

As shown in FIG. 5(b) and FIG. 6(b), for $t_{\rm AB}$=2.5 $\Delta$, as the temperature increases from $T$=0.1 $\Delta$ to $T\approx$ 1.5 $\Delta$, the concurrence drops abruptly from $C_{\rm AB}\approx$0.92 to $C_{\rm AB}$=0. The system is always in a mixed state of triplet and singlet. While at low temperature, the proportion of singlet is much larger than triplet and the spin-spin correlation between two dots is strong, leading to strong entanglement. When temperature is high, thermal fluctuations suppress the spin-spin correlation and thus entanglement becomes weak between two dots. Nonlocal correlation and entanglement mainly occur at low temperature region. FIG. 5(b) and FIG. 6(b) reflect similar conclusions to FIG. 2 and FIG. 4.

## IV. CONCLUDING REMARKS

To summarize, in this work we mainly studies the entanglement of the parallel-coupled DQDs by the HEOM approach. By analyzing the reduced density matrix as well as by properly constructing the Hamiltonian of the DQDs, we can obtain more precise information about quantum coherence, quantum correlation, and quantum entanglement. We quantitatively studied the influence of the coupling strength between DQDs and environment temperature on entanglement, and investigated the relationship of Rényi entropy between total system and subsystems.

As for two identical parallel-coupled dots, the quantum many-body effects result in different spin states in the DQDs, which have different effects on entanglement. There are two distinct quantum ground states in this kind of system, *i.e.*, the spin-1/2 state and the spin singlet between two dots. At low temperature and strong interdot coupling strength, quantum correlation and entanglement become stronger. The quantum mutual entropy also quantifies the quantum correlation. The second-order Rényi entropy provides a lower bound for the von Neumann entropy. The second-order Rényi entropy can reflect more information than the von Neumann entropy. Interesting results can be obtained by comparing the results for the combined effects of driving an electric or magnetic field on the DQD system. We hope that this work will encourage further efforts both theoretically and experimentally to probe the mechanism and many-body effects on entanglement of DQD system.

## V. ACKNOWLEDGMENTS

This work was supported by the Ministry of Science and Technology of China (No.2016YFA0400900 and No.2016YFA0200600), the National Natural Science Foundation of China (No.21573202 and No.21633006), the Fundamental Research Funds for the Central Universities (No.2340000074), The Supercomputing Center of USTC is gratefully acknowledged.

[1] M. A. Nielsen and I. L. Chuang, *Quantum Computation and Quantum Information*, Cambridge: Cambridge University Press, (2000).
[2] R. Islam, R. Ma, P. M. Preiss, M. E. Tai, A. Lukin, M. Rispoli, and M. Greiner, Nature **528**, 77 (2015).
[3] N. J. Cerf and C. Adami, Phys. Rev. Lett. **79**, 5194 (1997).
[4] E. Cocchi, L. A. Miller, J. H. Drewes, C. F. Chan, D. Pertot, F. Brennecke, and M. Köhl, Phys. Rev. X **7**, 031025 (2017).
[5] H. A. Engel, L. Kouwenhoven, D. Loss, and C. Marcus, Quantum Inf. Process. **3**, 115 (2004).
[6] Y. Okazaki, S. Sasaki, and K. Muraki, Phys. Rev. B **84**, 161305 (2011).
[7] S. Amasha, A. Keller, I. Rau, A. Carmi, J. Katine, H. Shtrikman, Y. Oreg, and D. Goldhaber-Gordon, Phys. Rev. Lett. **110**, 046604 (2013).
[8] D. Goldhaber-Gordon, H. Shtrikman, D. Mahalu, D. Abusch-Magder, U. Meirav, and M. Kastner, Nature **391**, 156 (1998).
[9] C. A. Büsser and F. Heidrich-Meisner, Phys. Rev. Lett. **111**, 246807 (2013).
[10] D. Loss and D. P. DiVincenzo, Phys. Rev. A **57**, 120 (1998).
[11] G. Burkard, D. Loss, and D. P. DiVincenzo, Phys. Rev. B **59**, 2070 (1999).
[12] C. H. Bennett and D. P. DiVincenzo, Nature (London) **404**, 247 (2000).
[13] T. Hatano, M. Stopa, and S. Tarucha, Science **309**, 268 (2005).
[14] A. Ramšak, J. Mravlje, R. Žitko, and J. Bonča, Phys. Rev. B **74**, 241305 (2006).
[15] H. Johannesson, D. F. Mross, and E. Eriksson, Mod. Phys. Lett. B **25**, 1083 (2011).
[16] J. S. Jin, X. Zheng, and Y. J. Yan, J. Chem. Phys. **128**, 234703 (2008).
[17] X. Zheng, J. Jin, and Y. Yan, New. J. Phys. **10**, 093016 (2008).
[18] X. Zheng, J. S. Jin, S. Welack, M. Luo, and Y. J. Yan, J. Chem. Phys. **130**, 164708 (2009).
[19] X. Zheng, Y. Yan, and M. Di Ventra, Phys. Rev. Lett. **111**, 086601 (2013).
[20] D. Hou, S. K. Wang, R. L. Wang, L. Z. Ye, R. X. Xu, X. Zheng, and Y. J. Yan, J. Chem. Phys. **142**, 104112 (2015).
[21] L. Ye, D. Hou, X. Zheng, Y. Yan, and M. Di Ventra, Phys. Rev. B **91**, 205106 (2015).

DOI:10.1063/1674-0068/31/cjcp1806138 

[22] L. Ye, X. Zheng, Y. Yan, and M. Di Ventra, Phys. Rev. B **94**, 245105 (2016).
[23] L. Z. Ye, X. L. Wang, D. Hou, R. X. Xu, X. Zheng, and Y. J. Yan, Wires. Comput. Mol. Sci. **6**, 608 (2016).
[24] P. W. Anderson, Phys. Rev. **124**, 41 (1961).
[25] J. Chen, A. Chang, and M. Melloch, Phys. Rev. Lett. **92**, 176801 (2004).
[26] J. Von Neumann, Mathematisch-Physikalische Klasse **1927**, 273 (1927).
[27] C. E. Shannon, ACM SIGMOBILE Mobile Compt. Comm. Rev. **5**, 3 (2001).
[28] A. Rényi, *On Measures of Entropy and Information*, in *Proceedings of the Fourth Berkeley Symposium on Mathematical Statistics and Probability, Volume 1: Contributions to the Theory of Statistics*, Berkeley, California: University of California Press, (1961).
[29] S. Goldstein and J. L. Lebowitz, Physica D **193**, 53 (2004).
[30] C. E. Shannon, Bell Labs Tech. J. **28**, 656 (1949).
[31] A. Daley, H. Pichler, J. Schachenmayer, and P. Zoller, Phys. Rev. Lett. **109**, 020505 (2012).
[32] J. Eisert, M. Cramer, and M. B. Plenio, Rev. Mod. Phys. **82**, 277 (2010).
[33] M. M. Wolf, F. Verstraete, M. B. Hastings, and J. I. Cirac, Phys. Rev. Lett. **100**, 070502 (2008).
[34] Z. H. Li, N. H. Tong, X. Zheng, D. Hou, J. H. Wei, J. Hu, and Y. J. Yan, Phys. Rev. Lett. **109**, 266403 (2012).
[35] L. Pan, Y. D. Wang, Z. H. Li, J. H. Wei, and Y. J. Yan, J. Phys.: Condens. Matter **29**, 025601 (2016).
[36] S. Hill and W. K. Wootters, Phys. Rev. Lett. **78**, 5022 (1997).
[37] S. Keßler, I. P. McCulloch, and F. Marquardt, New J. Phys. **15**, 053043 (2013).
[38] R. Horodecki, P. Horodecki, M. Horodecki, and K. Horodecki, Rev. Mod. Phys. **81**, 865 (2009).
[39] R. Horodecki and M. Horodecki, Phys. Rev. A **54**, 1838 (1996).
[40] F. A. Bovino, G. Castagnoli, A. Ekert, P. Horodecki, C. M. Alves, and A. V. Sergienko, Phys. Rev. Lett. **95**, 240407 (2005).
[41] W. G. Van der Wiel, S. De Franceschi, J. M. Elzerman, T. Fujisawa, S. Tarucha, and L. P. Kouwenhoven, Rev. Mod. Phys. **75**, 1 (2002).

**Xiao Zheng** obtained his Bachelor degree in Chemistry at University of Science and Technology of China (USTC) in 2002. Then he went to the University of Hong Kong for postgraduate study and received his Ph.D. degree in Chemistry there in 2007. Afterwards he moved to Hong Kong University of Science and Technology to carry out postdoctoral research. In 2008 he went to Duke University in United States first as a visiting scholar and then as a postdoctoral research associate. In 2010 he returned to China and joined the National Laboratory for Physical Sciences at the Microscale of USTC as an assistant professor, and then was promoted to full professor in 2015. Professor Zheng's research area is theoretical and computational chemistry. His research topics include development of theoretical methods for open quantum systems, development of accurate and efficient density functional theory methods, and development of first-principles simulation methods for novel materials with applications to nanoelectronics, photoenergy conversion, quantum information, and quantum computation.

DOI:10.1063/1674-0068/31/cjcp1806138 